Two-dimensional semiconducting nanocrystals for photocatalytic hydrogen production from water

Shintaro Ida

[1]*Department of Applied Chemistry, Faculty of Engineering, Kyushu University, Japan*
[2]*International Institute for Carbon-Neutral Energy Research (WPI-I^{2}CNER), Kyushu University, Japan*

Introduction

Hydrogen production using semiconducting photocatalysts such as NiO-loaded La-doped $NaTaO_3$ and $Rh_{2-y}Cr_yO_3$-loaded $(Ga_{1-x}Zn_x)(N_{1-x}O_x)$ has attracted attention as a clean solar hydrogen-generation system.[1, 2] High crystallinity and high surface area are important properties required for high efficiency photocatalysts. Two-dimensional semiconductor nanocrystal (nanosheet) prepared by exfoliation of layered metal oxides are ideal materials that can satisfy both of these requirements.[3-6] For instance, Pt-loaded $[Nb_6O_{17}]^{4-}$, Rh_2O_3-loaded $[Ca_2Nb_3O_{10}]^-$, and Pt-loaded $[Ca_2Nb_3O_{10}]^-$ nanosheets have been reported to exhibit high catalytic efficiency, where Pt and Rh_2O_3 act as co-catalysts.[3-5] The photocatalytic activity is strongly dependent on the co-catalyst and the loading method or process, so that a catalyst without co-catalyst or with too much co-catalyst has poor photocatalytic activity. The role of these co-catalysts is the introduction of active sites and the promotion of charge separation. Another method to improve the catalytic activity is doping with transition metals. For instance, doping of Zr into the lattice of NiO-loaded $KTaO_3$ is reported to improve the catalytic activity, where the metal doping is performed to control the concentration of electrons. However, the doping of only transition metals in a catalyst without co-catalyst loading does not generally cause a significant improvement in activity compared to that with co-catalyst loading. One reason for this could be that most of the dopants in bulk have only an indirect effect on the reaction on the surface, because almost all of the dopants are present within the catalyst, rather than on the catalyst surface. In contrast, all dopants in a nanosheet are present very close to the surface, because the thickness of the nanosheet is approximately 1 nm. Therefore, most of the dopants in a nanosheet can be expected to be directly involved in the catalytic reaction and cause a significant improvement in photocatalytic activity in the same manner as co-catalyst loading.

In this study, we report on the preparation and photocatalytic properties of Rh-doped oxide nanosheets, which exhibited high activity for H_2 production from a water/methanol system without co-catalyst loading.

Experimental

Nanosheet synthesis. Nanosheets were prepared by exfoliation of layered oxide. Rh-doped oxide nanosheets were prepared as follows. $KCa_2Nb_{3-x}Rh_xO_{10-\delta}$ (x = 0, 0.001, 0.01, 0.03, 0.1, 0.15) powder was prepared by a solution method. $KOOCCH_3$, $Ca(OOCCH_3)\cdot 0.5H_2O$, $RhCl_3\cdot 3H_2O$ and Nb_2O_5 were mixed at a ratio of 1.3:2:3-x:x in water, after which the water was evaporated by heat treatment. The mixture was calcined in air at 673 K for 2 h, followed by grinding and calcination at 1473 K for 10 h (x = 0, 0.001, 0.01, 0.03) and 1423 K for 1.5 h (x = 0.1, 0.15). $KCa_2Rh_xNb_{3-x}O_{10}$ (1.0g) was converted into the protonated form by acid-exchange processing several times using 5 M HNO_3 solution (100 mL). After proton exchange reaction, the powder was washed in several change of water by centrifugation process. The sediment (powder paste) obtained after centrifugation process was used to next treatment without drying treatment. A colloidal $Ca_2Nb_3O_{10}$ nanosheet suspension was obtained by stirring the paste of protonated power (0.2 g) in a 0.025 M tetrabutylammonium hydroxide (TBAOH) aqueous solution (50 mL) for one week (The accurate weight of the protonated powder was measured by drying the paste). The separation of unexfoliated power was carried out by spontaneous precipitation for 1 day and the supernatant was used as nanosheet suspension. The concentration of nanosheet was calculated from the powder obtained by drying the nanosheet suspension at 500 °C. The concentration of nanosheet suspension was around 1.0 - 2.5 mg/L.

Photocatalytic reactions. The photocatalytic decomposition of water was performed using a conventional closed circulating system. Nanosheet suspension containing 5 mg of nanosheet was added in 150 mL of aqueous 10 vol % methanol solution. A quartz reaction cell was irradiated by an external light source consisting of a 500W Xe lamp. During photodecomposition, the suspension was mixed using a magnetic stirring bar. Ar gas (initial pressure: 18.3 kPa) was used as the circulating carrier gas. The amounts of H_2 and O_2 formed were measured by gas chromatography with a thermal conductivity detector (Shimadzu Corp., GC-8A), which was connected to a conventional volumetric circulating line with a vacuum pump.

Determination of the quantum efficiency. The determination of the quantum efficiency for hydrogen generation was performed using the same closed circulating system under illumination of 300W Xe lamp with bandpass filter system. The light intensity was measured using a Si photodiode (Hamamatsu Photonics K.K., S2281). The total light intensities were 15.4 mW/s (300 nm), 16.3 mW/s (350 nm), and 52.6 mW/s (420 nm). The irradiation area was around 3.2-4.0 cm^2.

Characterization and Equipment. XRD patterns were collected by a Rigaku RINT-2500 diffractometer using monochromatized Cu Kα radiation. XP spectra were analyzed by Shimadzu AXIS 165. TEM was carried out using a JEOL JEM2400 microscope operating at 200kV. Langmuir-Blodgett film was manufactured by USI USI-3-22, and surface morphology analyzed by AFM (SII Nano navi 2).

Results and Discussion

Figure 1 shows the model of crystal structure of Rh-doped calcium niobate nanosheet prepared by exfoliating layered $KCa_2Nb_{3-x}Rh_xO_{10-\delta}$. Most of the RhO_6 units in the nanosheet can be in direct contact with the reactants. Exfoliation of the layered structure into individual nanosheets was confirmed by atomic force microscopy (AFM). In order to evaluate many nanosheets, a monolayer film of nanosheets was prepared on a Si substrate by the Langmuir-Blodgett (LB) method. A well-organized nanosheet film could be obtained when the surface pressure was 15 mN m^{-1}. Figure 2 shows an AFM image of the Rh(0.03)-doped Ca-Nb-O sheet film. The contrast of the nanosheets was homogeneous, and there were no particles on the nanosheets. The measured thickness of all the nanosheets was approximately 2.8-3.0 nm and the lateral size was ca. 1 μm. These observed thickness is about 1.5 nm larger than that of the theoretical perovskite blocks in the host solid. The thickness of the oxide nanosheets observed by AFM was generally larger than that estimated from crystallographic data, because of the absorption of water and amine, and other systematic factors in the AFM measurements.

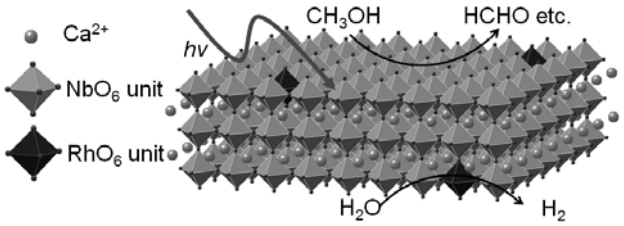

Figure 1. Model of crystal structure of Rh-doped calcium niobate nanosheet.

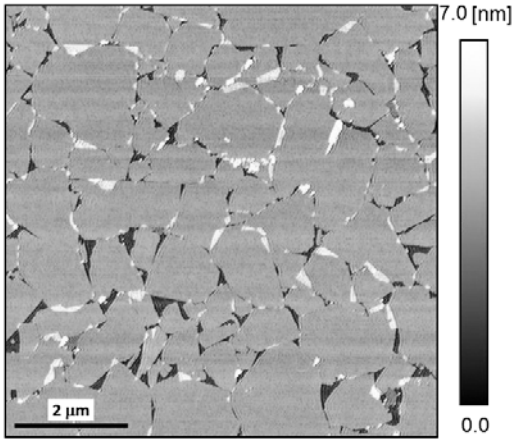

Figure 2. AFM image of the Rh(0.03)-doped Ca-Nb-O sheet film.

Figure 3 shows time courses of H_2 evolution from aqueous 10 vol% methanol solutions by photoirradiation in the presence of 5 mg of Rh(0.03)-doped Ca-Nb-O nanosheets, the protonated form of the nanosheets, and the parent layered oxide. All samples have no co-catalyst loading. The H_2 production rates of the parent layered oxide and the protonated form were very low, whereas the Rh-doped Ca-Nb-O sheets exhibited high photocatalytic activity. The H_2 production rate of the nanosheets (384.8 μmol/h) was 165 times larger than that of the parent rhodium-doped layered oxide (2.3 μmol/h). However, the non-doped Ca-Nb-O sheets did not exhibit such a dramatic improvement in photocatalytic activity. The H_2 production rate with the non-doped Ca-Nb-O sheets and the parent layered oxide were 21.0 and 1.6 μmol/h, respectively.

A model of the photocatalytic reaction mechanism in the presence of CH_3OH is illustrated in Fig. 1. CH_3OH is oxidized to formaldehyde, by photo-excited holes, whereas photo-excited electrons cause the reduction of H_2O to H_2. After reaction, HCHO (1610 μmol) was detected with formaldehyde as the main product due to the oxidation of methanol in Rh(0.03)-doped nanosheet system. Moreover, H_2 and D_2 evolution experiment using CD_3OD instead of CH_3OH resulted in a H_2/D_2 mass current ratio of approximately 500. In the cases of H_2O/CD_3OD system, CD_3OD was converted to CD_3OH after reaction, which is due to deuterium-hydrogen exchange between CD_3OD and H_2O. If the hydrogen evolved under illumination is due to decompositions of CD_3OD or CD_3OH, D_2 (mass 4) or HD (mass 3) should be detected. However, main peak for H_2O/CD_3OD system was mass 2 (H_2). This indicates that H_2 evolution is due to the reduction of H_2O.

Figure 4a shows the photocatalytic activity for H_2 production as a function of the amount of Rh doping. The Rh(0.03)-doped Ca-Nb-O sheet exhibited the maximum activity. The apparent quantum

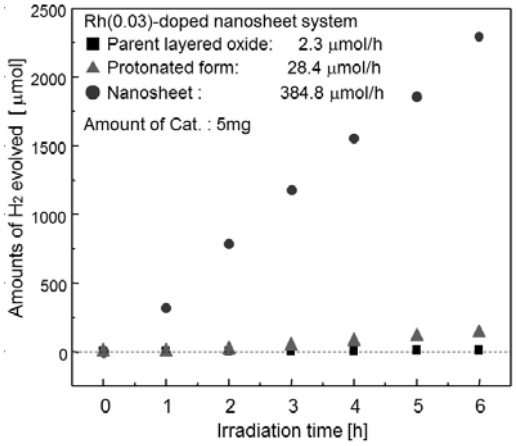

Figure 3. Time courses of H_2 evolution from aqueous 10 vol% methanol solutions by photoirradiation in the presence of 5 mg of Rh(0.03)-doped Ca-Nb-O system (500W Xe lamp).

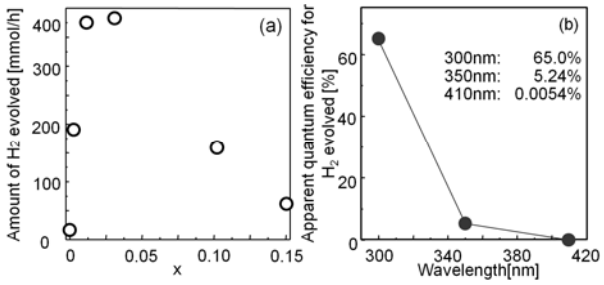

Figure 4. Photocatalytic activity for H_2 production as a function of the amount of Rh(x) doping in Ca-Nb-O nanosheet (a), and apparent quantum efficiency for H_2 generation and UV-vis spectrum for Rh(0.03)-doped Ca-Nb-O nanosheet (b). Reaction condition : 5 mg of catalyst, 150 cm^3 of aqueous 10 vol % methanol solution.

efficiency for H_2 production using Rh(0.03)-doped Ca-Nb-O sheet at 300 and 410 nm was 65.0 and 0.0054%, respectively, so that the apparent quantum efficiency was relatively high under UV-light illumination as shown in Fig. 4b.

In conclusion, Rh-doped Ca-Nb-O nanosheets exhibited high photocatalytic activity for H_2 production from a water/methanol system without co-catalyst loading. The apparent quantum efficiency at 300 nm was 65%. The doping of a noble metal into the nanosheet is a promising approach to improve the photocatalytic activity

Acknowledgment

This work was supported by JST PRESTO program.

References

1. Kato, H.; Asakura, K.; Kudo, A. *J. Am. Chem. Soc.* **2003**, *125*, 3082-3089.
2. Maeda, K.; Teramura, K.; Lu, D.; Takata, T.; Saito, N.; Inoue, Y.; Domen, K. *Nature* **2006**, *440*, 295.
3. Abe, R.; Shinohara, K.; Tanaka, A.; Hara, M.; Kondo, J. N.; Domen, K. *Chem. Mater.* **1997**, *9*, 2179-2184.
4. Hata, H.; Kobayashi, Y.; Bojan, V.; Youngblood, W. J.; Mallouk, T. E. *Nano Lett.* **2008**, *8*, 794-799.
5. Ebina, Y.; Sasaki, T.; Harada, M.; Watanabe, M. *Chem. Mater.* **2002**, *14*, 4390-4395.
6. Okamoto, Y.; Ida, S.; Hyodo, J.; Hagiwara, H.; Ishihara, T. *J. Am. Chem. Soc.*, **in press.**